Published in Optics Communications 89, issue 1, 5-11, 1992
which should be used for any reference to this work

TIR holography analyzed with coupled wave theory

P. Ehbets, H.P. Herzig and R. Dändliker
Institute of Microtechnology, University of Neuchâtel, Neuchâtel, Switzerland

A coupled wave model is presented to describe the diffraction behavior of thick total-internal reflection (TIR) holograms. We have transformed the coupled wave equations into a transfer matrix formalism, enabling a general treatment of the boundary conditions. The off-Bragg characteristic of TIR holograms is found to be completely different from normal volume holograms. The diffraction efficiency depends strongly on the phase of the total internal reflection and the optical pathlength through the hologram. High efficiency at the same angle as used for the recording requires careful control of all parameters.

1. Introduction

Total-internal reflection (TIR) holography offers a method to realize transmission holograms with object planes in the near-field. This holographic recording geometry was first investigated by Stetson [1] and has become of recent interest due to its applications to photolithography [2,3] and optical interconnects [4].

Fig. 1 shows the typical recording set-up for TIR holography. The object beam interferes with the reference beam, which is fed through a prism under 45° into the holographic layer and totally reflected at the film–air interface. The interface pattern of three beams, namely the object beam, the reference beam and the total internal reflection of the reference (TIR), is recorded in the holographic film. In general three thick diffraction gratings are formed. Two of them involve the object beam, while the third is a Lippmann grating formed by the interference of the reference with the TIR beam. The electric field vectors of the reference and the TIR beam are orthogonal for recording with p polarized light, therefore no Lippmann grating is formed.

We are interested in the conditions for replaying the object wave with high diffraction efficiency. Using coupled wave theory, we shall study the influence of the relative phases of the gratings, the phase shift due to total reflection at the backside, and the phase propagation through the hologram.

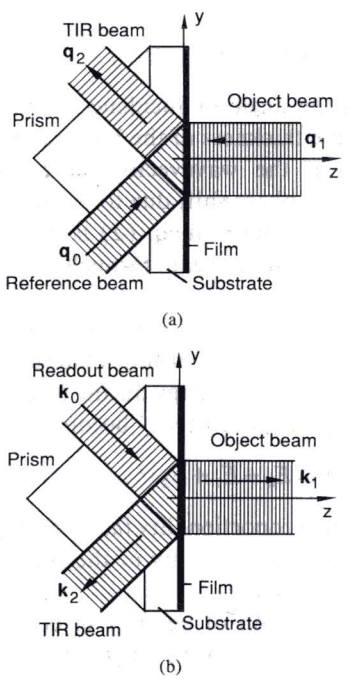

Fig. 1. (a) Recording and (b) readout geometry for TIR holography.

2. Coupled wave analysis

The following coupled wave model is developed for plane waves of infinite extent. The plane of incidence is the yz plane, as shown in fig. 1. At recording, three waves are present. They can be written as

$$\boldsymbol{E}_i(y, z) = A_i \boldsymbol{u}_i \exp[-\mathrm{i}(\boldsymbol{q}_i \cdot \boldsymbol{x} - \varphi_i)], \quad i = 0, 1, 2, \tag{1}$$

where $\boldsymbol{q}_i$ are the wavevectors at recording, A_i the real amplitudes, $\boldsymbol{u}_i$ the unity vectors in the direction of the polarizations, and φ_i the constant phase factors defined at $y = z = 0$. The index i denotes the reference wave ($i=0$), the object wave ($i=1$), and the TIR wave ($i=2$). Note that $A_2 = A_0$ and that for the s polarization $\boldsymbol{u}_i = (1, 0, 0)$.

Since the TIR beam is generated at the film–air interface, its constant phase at $y = z = 0$ is determined by

$$\varphi_2 = \varphi_0 + \Omega_{\mathrm{TIR}}(\theta) - 2\beta d \cos(\theta), \tag{2}$$

where θ is the angle of incidence of the reference wave, d is the thickness of the holographic film, β is the length of the wavevectors at recording and $\Omega_{\mathrm{TIR}}(\theta)$ is the phase shift due to the total reflection at $z = d$. The last term in eq. (2) is the propagation phase of the reference beam through the holographic film.

If we assume that there is no absorption and that the response of the recording material is proportional to the incident energy during exposure, the resulting dielectric permittivity becomes

$$\epsilon(y, z) = \epsilon_{\mathrm{a}} + \delta |\boldsymbol{E}_0 + \boldsymbol{E}_1 + \boldsymbol{E}_2|^2, \tag{3}$$

where δ is the proportionality factor and ϵ_{a} is the average dielectric permittivity of the recording material before exposure.

After substitution of eq. (1) in eq. (3) the recorded permittivity can be written as

$$\epsilon(y, z) = \epsilon_{\mathrm{a}} + \delta \sum_{i=0}^{2} A_i^2 + \sum_{i<j=1}^{2} \Delta\epsilon_{ij} \cos(\boldsymbol{K}_{ij} \cdot \boldsymbol{x} - \boldsymbol{\Phi}_{ij}). \tag{4}$$

Three gratings are recorded simultaneously. Their grating vectors $\boldsymbol{K}_{ij}$, relative phases $\boldsymbol{\Phi}_{ij}$ and modulation amplitudes $\Delta\epsilon_{ij}$ are given by

$$\boldsymbol{K}_{ij} = \boldsymbol{q}_i - \boldsymbol{q}_j,$$

$$\boldsymbol{\Phi}_{ij} = \varphi_i - \varphi_j, \quad i<j = 1, 2,$$

$$\Delta\epsilon_{ij} = 2\delta A_i A_j \boldsymbol{u}_i \cdot \boldsymbol{u}_j. \tag{5}$$

Note that for p polarization the effective modulation level is $\boldsymbol{u}_i \cdot \boldsymbol{u}_j$ times smaller than for s polarization. The recording process of the hologram changes the average value ϵ_{a} of the dielectric permittivity to a new average value ϵ'_{a}.

Furthermore, we have considered the possibility of shrinkage or swelling of the holographic film during processing. Since we do not exactly know the influence of thickness variations on the recorded permittivity, we have used a simple geometrical model. Shrinkage or swelling in the z-direction alters only the z-component of the grating vectors:

$$\boldsymbol{K}_{ij}^{y}|_{\mathrm{new}} = \boldsymbol{K}_{ij}^{y}|_{\mathrm{old}},$$

$$\boldsymbol{K}_{ij}^{z}|_{\mathrm{new}} = \left(\frac{1}{1+s}\right) \boldsymbol{K}_{ij}^{z}|_{\mathrm{old}}, \tag{6}$$

where s is the relative thickness variation and $s>0$ stands for swelling and $s<0$ for shrinkage.

At readout, the hologram is illuminated with the plane wave $\boldsymbol{k}_0$, as shown in fig. 1b. According to the criteria derived in ref. [5], the three gratings work in the Bragg diffraction regime and will reconstruct only one diffraction order of significant amplitude. Thus, we describe the electric field inside the hologram by

$$\boldsymbol{E}(y, z) = \sum_{i=0}^{2} B_i(z)\, \boldsymbol{u}_i \exp(-\mathrm{i}\boldsymbol{k}_i \cdot \boldsymbol{x}), \tag{7}$$

where the index $i=0$ stands for the readout beam, $i=1$ for the reconstructed object beam, and $i=2$ for the TIR of the readout beam. The coefficients $B_i(z)$ are complex amplitudes, which vary in the z-direction due to the coupling between the waves.

At recording (fig. 1), the wavevectors $\boldsymbol{q}_i$ are assumed to be in the (y, z)-plane, namely

$$\boldsymbol{q}_0 = \beta(0, \sin\theta, \cos\theta), \quad \boldsymbol{q}_1 = \beta(0, 0, -1),$$

$$\boldsymbol{q}_2 = \beta(0, \sin\theta, -\cos\theta), \tag{8}$$

where θ is the incidence angle of the reference wave. The hologram is reconstructed with the readout wave $\boldsymbol{k}_0 = \beta'(0, \sin\theta', \cos\theta')$, where θ' is the incidence

angle. For the choice of readout wave indicated in fig. 1b, $\theta' < 0$. Due to the change of the average dielectric permittivity ϵ_a, the length $\beta' = (2\pi\sqrt{\epsilon'_a})/\lambda$ is different from β at recording, even for the same wavelength λ. The directions of the reconstructed wavevectors $\boldsymbol{k}_i$ are then determined by the β-value method [6]:

$$k_1^y = k_0^y - K_{12}^y = \beta' \sin\theta' + \beta \sin\theta ,$$
$$k_1^z = \sqrt{\beta'^2 - (k_1^y)^2} ,$$
$$k_2^y = k_0^y - K_{02}^y = \beta' \sin\theta' ,$$
$$k_2^z = \sqrt{\beta'^2 - (k_2^y)^2} . \qquad (9)$$

The coupled wave equations are now derived by introducing the electric field, eq. (7), and the dielectric permittivity, eq. (4), into the wave equation

$$\Delta \boldsymbol{E}(y, z) + (2\pi/\lambda)^2 \epsilon(y, z)\, \boldsymbol{E}(y, z) = 0 . \qquad (10)$$

The modulation of the refractive index is assumed to be small, therefore the weak coupling approximation can be used [7]. We obtain the following coupled wave equations:

$$\frac{\mathrm{d}}{\mathrm{d}z} B_0 = -\mathrm{i} \frac{\kappa_{01}}{\cos\theta'} \exp[\mathrm{i}(\Delta k_{12} z + \Phi_{12})]\, B_1$$
$$-\mathrm{i} \frac{\kappa_{02}}{\cos\theta'} \exp[\mathrm{i}(\Delta k_{02} z + \Phi_{02})]\, B_2 ,$$
$$\frac{\mathrm{d}}{\mathrm{d}z} B_1 = -\mathrm{i}\kappa_{10} \exp[-\mathrm{i}(\Delta k_{12} z + \Phi_{12})]\, B_0$$
$$-\mathrm{i}\kappa_{12} \exp[\mathrm{i}(\Delta k_{01} z + \Phi_{01})]\, B_2 ,$$
$$\frac{\mathrm{d}}{\mathrm{d}z} B_2 = \mathrm{i} \frac{\kappa_{20}}{\cos\theta'} \exp[-\mathrm{i}(\Delta k_{02} z + \Phi_{02})]\, B_0$$
$$+\mathrm{i} \frac{\kappa_{21}}{\cos\theta'} \exp[-\mathrm{i}(\Delta k_{01} z + \Phi_{01})]\, B_1 , \qquad (11)$$

where θ' is the incidence angle of the readout beam $\boldsymbol{k}_0$. The off-Bragg factors are defined by

$$\Delta k_{12} = k_0^z - k_1^z - K_{12}^z ,$$
$$\Delta k_{02} = k_0^z - k_2^z - K_{02}^z ,$$
$$\Delta k_{01} = k_1^z - k_2^z - K_{01}^z . \qquad (12)$$

The z-components of the grating vectors $\boldsymbol{K}_{12}$ and the wavevectors $\boldsymbol{k}_i$ are obtained from eqs. (5), (8) and (9).

In the case of the special geometry shown in fig. 1, with $A_0 = A_2$, we found for the coupling coefficients in eq. (11) $\kappa_{01} = \kappa_{10} = \kappa_{12} = \kappa_{21} = \kappa_1$ and $\kappa_{02} = \kappa_{20} = \kappa_2$, with

$$\kappa_1 = \beta' \Delta\epsilon_{01}/4\epsilon'_a , \quad \kappa_2 = \beta' \Delta\epsilon_{00}/4\epsilon'_a , \qquad (13)$$

for the s polarization and

$$\kappa_1 = (\beta' \Delta\epsilon_{01}/4\epsilon'_a)\boldsymbol{u}'_0 \cdot \boldsymbol{u}'_1 , \quad \kappa_2 = 0 , \qquad (14)$$

for the p polarization. In addition to the coupled wave equations (11), the components of the electric field in eq. (7) must satisfy the following boundary conditions for $z = 0$ and $z = d'$:

$$B_0(0) = \exp(\mathrm{i}\varphi'_0) ,$$
$$B_1(0) = 0 ,$$
$$B_2(d') = B_0(d') \exp\{\mathrm{i}[\Omega_{\mathrm{TIR}}(\theta') - 2\beta' d' \cos(\theta')]\} , \qquad (15)$$

where $\Omega_{\mathrm{TIR}}(\theta')$ is the phase shift of the total internal reflection, and d' is the thickness of the hologram after processing.

The influence of the different phase factors φ_q can be seen more clearly when the complex amplitudes B_p are substituted by

$$C_p(z) = B_p(z) \exp(\mathrm{i}\varphi_q) , \quad p, q = 0, 2; 1, 1; 2, 0 . \qquad (16)$$

From eq. (11) we get the new coupled wave equations

$$(\mathrm{d}/\mathrm{d}z) C_0 = -\mathrm{i}(\kappa_1/\cos\theta') \exp(\mathrm{i}\Delta k_{12} z) C_1$$
$$-\mathrm{i}(\kappa_2/\cos\theta') \exp(\mathrm{i}\Delta k_{02} z) C_2 ,$$
$$(\mathrm{d}/\mathrm{d}z) C_1 = -\mathrm{i}\kappa_1 \exp(-\mathrm{i}\Delta k_{12} z) C_0$$
$$-\mathrm{i}\kappa_1 \exp(\mathrm{i}\Delta k_{01} z) C_2 ,$$
$$(\mathrm{d}/\mathrm{d}z) C_2 = \mathrm{i}(\kappa_2/\cos\theta') \exp(-\mathrm{i}\Delta k_{02} z) C_0$$
$$+\mathrm{i}(\kappa_1/\cos\theta') \exp(-\mathrm{i}\Delta k_{01} z) C_1 . \qquad (17)$$

The coupled wave equations (17) are now independent of the relative phases $\Phi_{pq} = \varphi_p - \varphi_q$ of the gratings. The relevant phase information is grouped in the new boundary conditions, obtained from eq. (15),

$$C_0(0) = \exp[\mathrm{i}(\varphi'_0 + \varphi_2)] ,$$

$$C_1(0)=0\,,$$

$$C_2(d')=C_0(d')\exp(\mathrm{i}\Delta\psi)\,, \tag{18}$$

with $\Delta\psi=\Omega_{\mathrm{TIR}}(\theta')-\Omega_{\mathrm{TIR}}(\theta) \quad -2[\beta' d'\cos(\theta') -\beta d\cos(\theta)]$.

The constant phase $\varphi_0'+\varphi_2$ of the coefficient C_0, describing the readout beam at $z=0$, has no importance, because it causes only a common phase shift of the three waves. The phase $\Delta\psi$ of the coefficient C_2 at $z=d'$, however, has a strong influence on the solutions, because it changes the phase relation between the waves. The phase shift $\Delta\psi$ is due to differences between recording and readout, i.e. the phase change of the total internal reflection and the change of the optical length through the hologram.

3. Transfer matrix for numerical solutions

For the numerical solution of the coupled wave equations (17), we have used a transfer matrix formalism. The advantage of this approach is that the coupled wave system can be easily combined with other transfer matrices. This allows to calculate the integration of the TIR hologram in a more complex system. In addition, the transfer matrix is independent of the boundary conditions. This allows a general treatment of possible boundary conditions, without being obliged to integrate the coupled wave equations again.

The coupled wave equations (17) represent a linear system of differential equations for the unknown coefficients $C_i(z)$. Such a system can be described by a transfer matrix $\mathbf{M}_{pq}$, that transforms an input vector $\boldsymbol{C}(0)=(C_0(0), C_1(0), C_2(0))$ at $z=0$ into an output vector $\boldsymbol{C}(d')$ at $z=d'$, namely

$$\boldsymbol{C}(d')=[\mathbf{M}_{pq}]\cdot\boldsymbol{C}(0)\,, \quad p,q=0,1,2\,. \tag{19}$$

The transfer matrix $\mathbf{M}_{pq}$ can be derived by integrating the system of differential equations (17) for three different orthogonal boundary conditions at $z=0$, namely $\boldsymbol{C}(0)=(1,0,0)$, $(0,1,0)$ and $(0,0,1)$. Each solution $\boldsymbol{C}(d')$ defines then one column of the transfer matrix $[\mathbf{M}_{pq}]$. The differential equations (17) were integrated numerically by a Runge–Kutta algorithm.

We are finally interested in the diffraction efficiency, defined by

$$\eta_1=\frac{k_1^z}{k_0^z}\frac{|C_1(d')|^2}{|C_0(0)|^2}\,, \tag{20}$$

which is the fraction of the incident power coupled into the reconstructed object beam. The substitution of the boundary conditions (18) into eq. (20) yields for $C_0(0)=1$

$$\eta_1=\frac{k_1^z}{k_0^z}\left|M_{10}+M_{12}\left(\frac{M_{00}-M_{20}\exp(-\mathrm{i}\Delta\psi)}{M_{02}-M_{22}\exp(-\mathrm{i}\Delta\psi)}\right)\right|^2. \tag{21}$$

4. Discussion of the results

The figs. 2 to 4 present the diffraction efficiency, calculated from eq. (21), as a function of the readout angle θ', for both s and p polarized light. We have considered different values for the thickness variation, namely no shrinkage (fig. 2), 1% shrinkage (fig. 3), and 1% swelling (fig. 4). For all calculations the

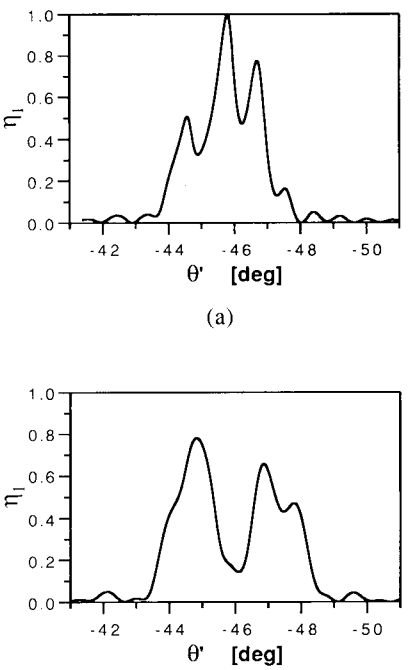

Fig. 2. Diffraction efficiency η_1 versus readout angle θ' for 0% shrinkage. (a) s polarization, (b) p polarization.

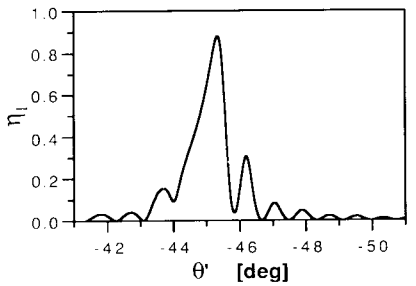

(a)

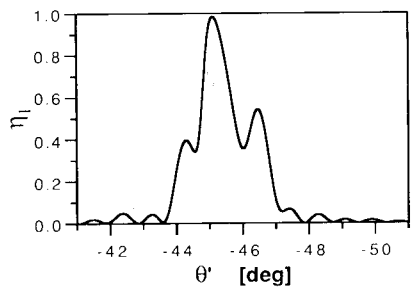

(b)

Fig. 3. Diffraction efficiency η_1 versus readout angle θ' for 1% shrinkage. (a) s polarization, (b) p polarization.

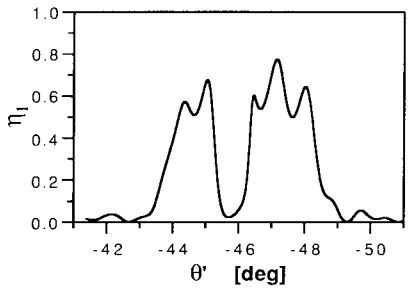

(a)

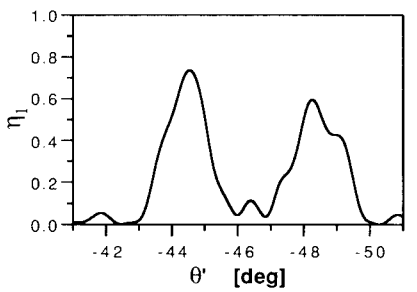

(b)

Fig. 4. Diffraction efficiency η_1 versus readout angle θ' for 1% swelling. (a) s polarization, (b) p polarization.

following parameters have been used: $\lambda = 0.488$ μm, $n_a = \sqrt{\epsilon_a} = 1.5$, $d = 15$ μm, $\theta = 45°$, and $A_0 = A_1$, which means equal intensity for the reference and the object beams. We have assumed the same value for the coupling factor κ_1 for both s and p polarization. This means for an interbeam angle of 45°, following eqs. (13) and (14), that the exposure has to be two times higher for p polarization than for s polarization. Therefore a modulation level of $\Delta\epsilon_{01} = 2\delta(A_0)^2 = 0.026$ for s polarization and $\Delta\epsilon_{01} = 2\delta(A_0)^2 \cos(\theta) = 0.037$ for p polarization has been chosen. The change of the average dielectric permittivity is calculated following eq. (4), using the same proportionality factor δ as for the exposure of the gratings. The resulting values for the refractive index are $n'_a = 1.51$ for s polarization and $n'_a = 1.53$ for p polarization.

A key element is the Lippmann grating $\boldsymbol{K}_{02}$, which couples light directly from the readout beam into the TIR beam. This grating is only present in the case of s polarization. This is the main reason for the differences between the results for p and s polarization.

The amplitude of the object beam $\boldsymbol{k}_1$ is coupled to the readout beam $\boldsymbol{k}_0$ and to the TIR beam $\boldsymbol{k}_2$ through the gratings $\boldsymbol{K}_{12}$ and $\boldsymbol{K}_{01}$, respectively. These two contributions are added coherently. Therefore the phase shift $\Delta\psi$ between the readout beam and the TIR is important. The phase shift $\Delta\psi$ is determined by the boundary condition of the hologram at $z = d'$, given by eq. (18). In figs. 2 to 4 we see rapid variations of the diffraction efficiency with the readout angle θ'. This can be explained by the angular dependence of $\Delta\psi$. For $\Delta\theta' = 1°$ the phase shift $\Delta\psi$ changes by more than 2π.

In the ideal case, i.e. if the recording and the readout parameters are identical, the Bragg angle for high diffraction efficiency is $\theta' = -45°$. Shrinkage or swelling (figs. 3 and 4), and also the change of the average permittivity ϵ'_a (figs. 2, 3 and 4), shift the Bragg angles at readout. The shift is different for the three gratings $\boldsymbol{K}_{ij}$. Large shrinkage or swelling will separate the angular regions where the gratings $\boldsymbol{K}_{01}$ and $\boldsymbol{K}_{12}$ are efficient, and therefore the influence of the coherent grating coupling will diminish. The out-

put of the hologram becomes insensitive to the phase shift $\Delta\psi$. This can already be seen in the case of 1% swelling in fig. 4. It shows two separated efficiency peaks centered at the shifted Bragg angles of the gratings $\boldsymbol{K}_{12}$ (left) and $\boldsymbol{K}_{01}$ (right). For readout angles near to one of the shifted Bragg angles only the corresponding grating will be efficient and as a consequence complete power transfer into the object beam should be possible. Using Kogelnik's two wave model [7], we can calculate the optimum modulation level $\Delta\epsilon_{01}$ for the transmission grating $\boldsymbol{K}_{12}$ at the shifted Bragg angle θ'. For 1% swelling we get $\theta' = -44.6°$ and $\Delta\epsilon_{01} = 0.042$ for s polarization, respectively $\theta' = -44.3°$ and $\Delta\epsilon_{01} = 0.058$ for p polarization. Fig. 5 shows that for this modulation level at the shifted Bragg angle all the incident power is transferred to the object beam ($\eta_1 = 1$).

For many practical applications, the object beam is not a plane wave but a focused beam or a more complex structure [2–4]. In these cases it is important that the object can be replayed at the same angle, because any change would introduce aberrations. It is difficult to record a hologram without a change of the average permittivity ϵ'_a, and therefore without a shift of the Bragg angle. Fortunately, as shown in fig. 3, it seems to be possible to compensate this shift by an appropriate shrink. The highest efficiency is again achieved near $\theta' = -45°$.

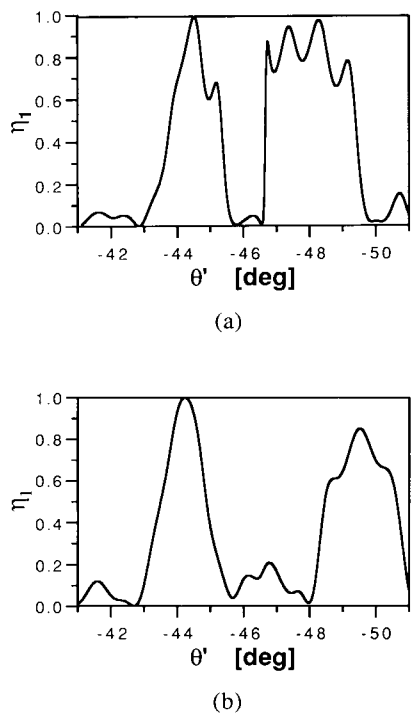

Fig. 5. Diffraction efficiency η_1 versus readout angle θ' for 1% swelling. Optimized transmission grating $\boldsymbol{K}_{12}$. (a) s polarization, (b) p polarization.

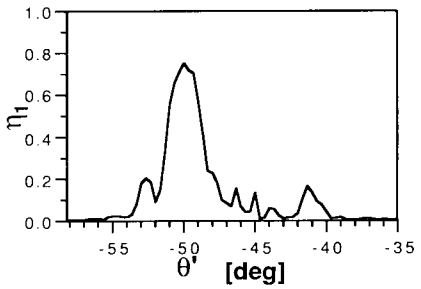

Fig. 6. Measured diffraction energy η_1 versus readout angle θ'. Material: photopolymer HRS 352, $d \approx 16$ µm, s polarization.

Actually, we have recorded only some few TIR holograms in dichromated gelatine and photopolymer. For the recording we have used the same geometry and the same parameters as for the numerical results. Fig. 6 shows the measured off-Bragg characteristics of a TIR hologram recorded in photopolymer. We observe a high Bragg peak with efficiency $\eta_1 \approx 80\%$ at $\theta' = -50°$ and a second smaller one at $\theta' = -41.5°$. The large shift of the Bragg angles indicates that during processing the thickness and the average permittivity have changed considerably. It is rather astonishing in comparison to figs. 4 and 5 that the second Bragg peak is much smaller than the first one. The main problem for quantitative comparison of theoretical and experimental results is the lacking detailed knowledge of the behavior of the holographic materials during recording and processing.

5. Conclusions

We have presented a coupled wave model, which allows to simulate the diffraction behavior of TIR holograms. For the numerical solution of the coupled wave equations we have used a transfer matrix formalism. This allows to separate the integration of the coupled wave equations and the treatment of the

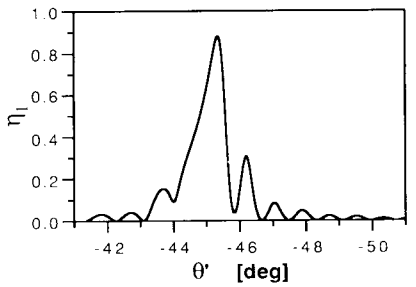

(a)

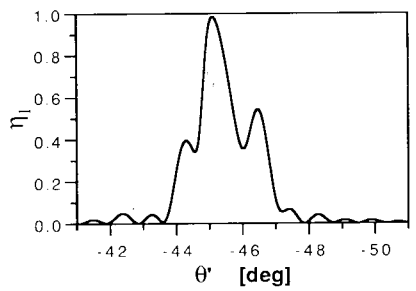

(b)

Fig. 3. Diffraction efficiency η_1 versus readout angle θ' for 1% shrinkage. (a) s polarization, (b) p polarization.

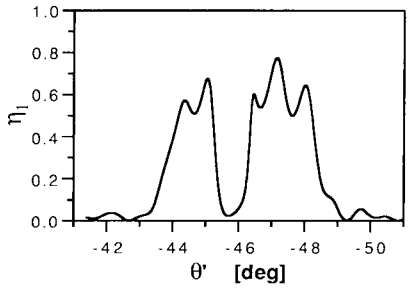

(a)

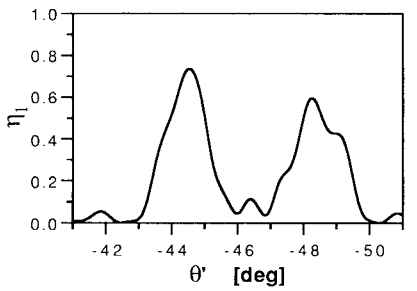

(b)

Fig. 4. Diffraction efficiency η_1 versus readout angle θ' for 1% swelling. (a) s polarization, (b) p polarization.

following parameters have been used: $\lambda = 0.488$ μm, $n_a = \sqrt{\epsilon_a} = 1.5$, $d = 15$ μm, $\theta = 45°$, and $A_0 = A_1$, which means equal intensity for the reference and the object beams. We have assumed the same value for the coupling factor κ_1 for both s and p polarization. This means for an interbeam angle of 45°, following eqs. (13) and (14), that the exposure has to be two times higher for p polarization than for s polarization. Therefore a modulation level of $\Delta\epsilon_{01} = 2\delta(A_0)^2 = 0.026$ for s polarization and $\Delta\epsilon_{01} = 2\delta(A_0)^2 \cos(\theta) = 0.037$ for p polarization has been chosen. The change of the average dielectric permittivity is calculated following eq. (4), using the same proportionality factor δ as for the exposure of the gratings. The resulting values for the refractive index are $n'_a = 1.51$ for s polarization and $n'_a = 1.53$ for p polarization.

A key element is the Lippmann grating $\boldsymbol{K}_{02}$, which couples light directly from the readout beam into the TIR beam. This grating is only present in the case of s polarization. This is the main reason for the differences between the results for p and s polarization.

The amplitude of the object beam $\boldsymbol{k}_1$ is coupled to the readout beam $\boldsymbol{k}_0$ and to the TIR beam $\boldsymbol{k}_2$ through the gratings $\boldsymbol{K}_{12}$ and $\boldsymbol{K}_{01}$, respectively. These two contributions are added coherently. Therefore the phase shift $\Delta\psi$ between the readout beam and the TIR is important. The phase shift $\Delta\psi$ is determined by the boundary condition of the hologram at $z = d'$, given by eq. (18). In figs. 2 to 4 we see rapid variations of the diffraction efficiency with the readout angle θ'. This can be explained by the angular dependence of $\Delta\psi$. For $\Delta\theta' = 1°$ the phase shift $\Delta\psi$ changes by more than 2π.

In the ideal case, i.e. if the recording and the readout parameters are identical, the Bragg angle for high diffraction efficiency is $\theta' = -45°$. Shrinkage or swelling (figs. 3 and 4), and also the change of the average permittivity ϵ'_a (figs. 2, 3 and 4), shift the Bragg angles at readout. The shift is different for the three gratings $\boldsymbol{K}_{ij}$. Large shrinkage or swelling will separate the angular regions where the gratings $\boldsymbol{K}_{01}$ and $\boldsymbol{K}_{12}$ are efficient, and therefore the influence of the coherent grating coupling will diminish. The out-

boundary conditions. The transfer matrix representation of the coupled wave solution can also be used to calculate the behavior of the hologram in a more complex system.

In general, three gratings are recorded in a TIR hologram, except for the case of p polarization and 90° between the reference and the TIR beam. Nevertheless, high diffraction efficiency can be achieved in all cases. However, the efficiency depends strongly on the change of the refractive index (average permittivity), of the hologram thickness (shrinking or swelling), and of the incidence angle of the reference beam. The main influence results from the change $\Delta\psi$ of the total phase shift between incident and TIR beam at the film–air interface (eq. 18)). It has two contributions: the phase of the total internal reflection and the optical path length of the TIR through the hologram. The consequence of this phase shift are rapid variations in the efficiency.

For practical applications, the object has to be replayed at the same angle as the recording was done, otherwise aberrations occur [4]. However, any variations of the recording parameters introduce a shift of the Bragg angle and reduce the efficiency, therefore it is important to control exactly the changes of the average permittivity and the hologram thickness during processing. The simulations show that conditions can be found, where the angular shifts due to these changes can compensate each other and efficient readout at the original recording angle can be obtained. Experiments in photopolymers and DCG show efficiency curves similar to the calculated results.

References

[1] K. Stetson, Appl. Phys. Lett. 11 (1967) 225.
[2] J. Brook and R. Dändliker, Microelectron. Eng. 11 (1990) 127.
[3] R.T. Chen, L. Sadovnik, T.M. Aye and T. Jannson, Optics Lett. 15 (1990) 869.
[4] D. Prongué and H.P. Herzig, Proc. SPIE 1281 (1990) 113.
[5] M.G. Moharam, T.K. Gaylord and R. Magnusson, Optics Comm. 32 (1980) 14.
[6] R.R.A. Syms, Practical volume holography (Oxford University Press, Oxford, 1990) p. 45.
[7] H. Kogelnik, Bell Syst. Tech. J. 48 (1969) 2909.